Available online at www.sciencedirect.com
ScienceDirect
Nuclear Instruments and Methods in Physics Research A 580 (2007) 919–924
NUCLEAR INSTRUMENTS & METHODS IN PHYSICS RESEARCH Section A
www.elsevier.com/locate/nima

Recent advances and future advances in time-of-flight PET

William W. Moses*

Lawrence Berkeley National Laboratory, 1 Cyclotron Road, Berkeley, CA 94720, USA

Available online 28 June 2007

Abstract

Simple theory predicts that the statistical noise variance in positron emission tomography (PET) can be reduced by an order of magnitude by using time-of-flight (TOF) information. This reduction can be obtained by improving the coincidence timing resolution, and so would be achievable in clinical, whole-body studies using with PET systems that differ little from existing cameras. The potential impact of this development is large, especially for oncology studies in large patients, where it is sorely needed. TOF PET was extensively studied in the 1980s but died away in the 1990s, as it was impossible to reliably achieve sufficient timing resolution without sacrificing other important PET performance aspects, such as spatial resolution and efficiency. Recent advances in technology (scintillators, photodetectors, and high-speed electronics) have renewed interest in TOF PET, which is experiencing a rebirth. However, there is still much to be done, both in instrumentation development and evaluating the true benefits of TOF in modern clinical PET. This paper looks at what has been accomplished and what needs to be done before TOF PET can reach its full potential.
Published by Elsevier B.V.

PACS: 87.58.Fg; 87.58.Pm; 81.70.Tx; 29.40.Me

Keywords: Positron emission mammography; Breast cancer; PEM camera design and optimization

1. Introduction

Like most imaging modalities, positron emission tomography (PET) is limited by statistical noise. By accurately measuring the arrival time of the two 511 keV positron annihilation photons in the ring of detectors that surrounds the patient, the location of the positron can be constrained. While this constraint is not tight enough to improve the spatial resolution, it can significantly reduce the statistical noise in the reconstructed images. This technique is known as time-of-flight (TOF) PET.

A number of PET cameras incorporating TOF measurement were built in the 1980s [1–8]. These cameras achieved timing resolution of ~500 ps and demonstrated the anticipated improvement in statistical noise, but their performance was limited by the materials and technologies available at that time. The scintillator used was BaF_2 or CsF. The fast emissions from BaF_2 are in the ultraviolet (UV) region, necessitating quartz-windowed photomultiplier tubes (PMTs), while CsF must be carefully packaged because it is extremely hygroscopic and its light output is so low that it has poor energy resolution and cannot be used for block detectors [9]. Both have worse spatial resolution and detection efficiency than BGO. In addition, TOF PET cameras required additional electronics to perform the TOF measurement, and those electronics had a tendency to "drift" over periods of hours or days. This forced design compromises that made TOF PET cameras to have overall inferior performance to non-TOF PET cameras, causing development of TOF PET to gradually die out [10].

New technologies and materials have become available in recent years and TOF PET cameras are once again being made. While this new generation of TOF PET cameras has fewer compromises than the previous generation, the ultimate performance has not yet been achieved. This paper looks at both the improvements that enabled the new generation of TOF PET cameras and what needs to be done before TOF PET can reach its full potential.

*Tel.: +1 510 486 4432; fax: +1 510 486 4768.
E-mail address: wwmoses@lbl.gov

0168-9002/$ - see front matter Published by Elsevier B.V.
doi:10.1016/j.nima.2007.06.038

2. Statistical noise in PET

In conventional PET, the location of an individual positron is constrained to lie along a line, and tomographic reconstruction algorithms then determine the three-dimensional (3D) source distribution. Even before computed tomography was applied to positron imaging to create what is now known as PET [11,12], it was realized that the 3D location of each positron could be determined by accurately measuring the difference in arrival times of the two annihilation photons [13]. In other words, the position of the positron would be constrained to a point rather than a line, so 3D images could be obtained without a reconstruction algorithm. However, the position along the line is localized to

$$\Delta x = \frac{c}{2}\Delta t \tag{1}$$

where Δx is the position error, c is the speed of light, and Δt is the error in the timing measurement. To get sub-centimeter position resolution, timing resolution of less than 50 ps is necessary, which is impossible to obtain. An achievable timing resolution (500 ps) constrains the positron position to a line segment ~7.5 cm long. While constraining the positron position to a line segment 7.5 cm long does not improve the spatial resolution, it does reduce the statistical noise in the reconstructed image if the line segment is shorter than the size of the emission source [14–16]. This multiplicative reduction factor f (corresponding to the reduction in noise variance) is given by

$$f = \frac{D}{\Delta x} = \frac{2D}{c\Delta t} \tag{2}$$

where D is the size of the emission source. For organs the size of the brain ($D \approx 20$ cm), this factor is greater than unity (implying some noise reduction) for timing resolution <1.3 ns. For whole-body imaging, the object size is larger ($D \approx 35$ cm) and $f>1$ for timing resolution <2.3 ns.

The mechanism by which noise is reduced by TOF is as follows. Consider a single point source in the field of view of a PET camera, such as in Fig. 1a. When that point source is imaged by collecting N coincident events, one would naively expect that image intensity for that voxel would be N and the statistical noise to be given by counting statistics, and so would be equal to sqrt(N). In this simple case, this estimate is correct.

Now consider what happens when a second point source that provides M coincident events is also placed in the field of view. With conventional PET the fundamental datum is a chord—a line joining the two detector elements that simultaneously observe 511 keV photons. The chord that joins the two point sources will have statistical fluctuations not only from the N counts of the source whose activity we would like to quantify, but also the M counts from the "background" source. In short, the voxels are coupled, and

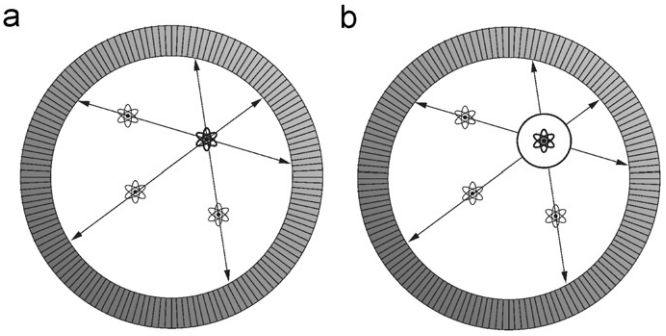

Fig. 1. Mechanism of TOF noise reduction. (a) In conventional PET, the fundamental measurement is the number of counts in a crystal–crystal pair, so the measurement of the activity in one voxel is coupled with the measurement of the activity in all other voxels. (b) In TOF PET, timing information can be used to remove the coupling between voxels that are separated by more than the TOF measurement distance.

while the reconstruction algorithm can decouple them to form an image with the correct average number of counts in each voxel, the statistical noise is increased and so is greater than sqrt(N). As any two voxels are connected by a chord, activity anywhere in the field of view increases the noise for every other voxel.

Reconstruction algorithms that include TOF information can reduce this coupling and so reduce the statistical noise. If the distance between two voxels is greater than the distance that TOF constrains the position to ($c\Delta t/2$), then the voxels essentially become uncoupled. With TOF reconstruction, coincident events contribute only to pixels near (i.e., within a distance consistent with the timing resolution) the target pixel, therefore the statistical fluctuations from the data contribute to a smaller number of image pixels. This concept is illustrated in Fig. 1b and is used to derive the variance reduction in Eq. (2). While the noise reduction is easily predicted for simple, uniform distributions, the improvement depends on the radioisotope distribution, which is rarely homogeneous. However, Eq. (2) provides a convenient approximation, which indicates that the noise variance reduction increases linearly with increasing patient "diameter" and decreasing coincidence timing resolution.

3. Recent and future advances

3.1. Scintillators

The key advance that enabled modern TOF PET was the development of new scintillator materials. The first developed was lutetium orthosilicate (LSO) or Lu_2SiO_5:Ce scintillator, which was discovered in 1991 [17]. Its properties are shown in Table 1, and it was immediately recognized that these properties are very attractive for PET. It has a very similar attenuation length to BGO but a considerably faster decay time (reducing dead time) and considerably higher light output (making block decoding easier). Several materials have similar chemical

Table 1
Comparison of scintillation properties for scintillators that have been used for PET as well as newly developed scintillator materials appropriate for TOF PET

Scintillator material	Luminosity (photons/MeV)	Decay time (ns)	Initial rate (photon/ns/MeV)	Coincidence timing resolution (w/BaF_2)	Energy resolution (%)	Attenuation length (cm)
BGO ($Bi_4Ge_3O_{12}$)	700	60	12	3 ns (lab) [30]	12	1.1
	7500	300	25	6 ns (PET) [31,32]		
Total	8200		37			
BaF_2	1800	0.8	2250	<200 ps (lab) [33,34]	10	2.3
	10,000	630	16	500 ps (PET) [10, 35]		
Total	11,800		2266			
CsF	2500	2.9	862	400 ps (lab) [36]	20	2.7
				500 ps (PET) [2,4]		
GSO (Gd_2SiO_5:Ce)	10,000	43 fall	232	965 ps (lab) [37]	9	1.5
		14.4 rise				
LSO (Lu_2SiO_5:Ce)	25,000	37	676	225 ps (lab) [18]	10	1.2
				1.2 ns (PET) [38]		
LuAP ($LuAlO_3$:Ce)	5800	11	524			
	2500	28	104	360 ps (lab) [39]	8	1.1
	1200	835	1			
Total	9500		629			
$LaCl_3$:Ce	50,000	20	2500	(218 ps)	3	2.9
$LaBr_3$:5% Ce	60,000	15	4000	260 ps (lab) [40]	3	2.2
				315 ps (PET) [23]		
$LaBr_3$:10% Ce	56,000	16	3500	(103 ps)	3	2.2
$LaBr_3$:20% Ce	55,000	17	3235	(94 ps)	3	2.2
$LaBr_3$:30% Ce	55,000	18	3056	(69 ps)	3	2.2
$CeBr_3$	68,000	17	4000	(129 ps)	3	2.2
LuI_3:Ce	100,000	23	4348	(125 ps)	4	1.8

When possible, timing resolution is quoted both for laboratory systems optimized for timing (“lab”) and for PET cameras (“PET”). Those materials above the heavy line are in reasonable scale commercial production, while those below are not yet commercially available. The number in parentheses in the coincidence timing resolution column is the expected timing for a pair of scintillator crystals of that material, based on measurements of single crystals in coincidence with BaF_2 scintillator.

composition and scintillation properties as LSO, such as MLS, LGSO, LYSO, and LPS. The high initial rate in Table 1 suggests that LSO should also have excellent timing properties. This prediction is born out in systems optimized for timing, as $\leqslant$225 ps FWHM coincidence timing has been obtained with 511 keV excitation [18,19]. Equally important for PET, LSO does not have the long attenuation length that degraded the performance of BaF_2- and CsF-based TOF PET cameras. A commercial LYSO-based PET camera with TOF capability (~600 ps coincidence timing resolution) has recently been released by Philips.

Another attractive, recently developed scintillator material for TOF is lanthanum bromide doped with 5% cerium [20], and a research TOF PET camera with $4 \times 4 \times 30\,mm^3$ crystals arranged in an 84 cm ring diameter and a 25 cm axial extent has recently been built [21]. With prototype detector modules, they have achieved 310–350 ps FWHM coincidence timing resolution, depending on the position [22,23]. Although the trade-offs when using $LaBr_3$ are different than those for LSO, Monte Carlo simulations of this design also predict very large improvements in imaging performance [21,24]. Indeed, the preliminary results from the completed camera show significant noise reduction, even though the measured timing resolution for the camera is “only” 475 ps FWHM [25]. With both the LYSO and $LaBr_3$:5%Ce cameras, significant performance improvement is observed experimentally.

While these two materials have enabled modern TOF PET, significant improvements in scintillator material properties are still possible. There are also some newly discovered materials that are quite promising for TOF PET. These materials are $LaBr_3$:Ce with cerium concentrations other than 5% [26], $CeBr_3$ [27], and LuI_3:Ce [28]. These new scintillator materials are truly astounding. All of them have light output that is at least 150% that of NaI:Tl, energy resolution (at 662 keV) that is better than 4% FWHM, and timing resolution that is better than barium fluoride. $LaBr_3$:30%Ce achieves timing resolution that is a factor of 2 better than that of BaF_2 (69 ps for a single crystal, implying 100 ps FWHM coincidence timing) [26,29]. However, LuI_3:Ce stands out even among these remarkable new materials. It has a light output of 100,000 photons/MeV (2.6 times that of NaI:Tl), energy

resolution of 4% FWHM (2.5 times better than LSO), and coincidence timing resolution of 125 ps FWHM (better than BaF_2)!

The choice of scintillator material affects the PET camera performance in many ways, and almost always involves trade-offs. Good energy resolution reduces background from Compton scatter in the patient. The photoelectric fraction and attenuation length affect the coincidence efficiency. A material with relatively low photoelectric fraction is unlikely to have both annihilation photons deposit >350 keV in the camera, thus reducing the coincidence efficiency. Ref. [41] simulates an 82 cm diameter PET camera made with three attenuation length deep crystals of each of the materials in Table 1. While LuI_3 has an efficiency that is 81% of LSO, the efficiency for $LaBr_3$ and $CeBr_3$ is 47% of LSO and that for $LaCl_3$ is 40% of LSO. The spatial resolution (particularly radial elongation) is also degraded by low photoelectric fraction and long attenuation length. Ref. [41] predicts the FWHM of the point spread function as a function of the distance from the center of the tomograph ring. BGO, LSO, LuAP, LuYAP, and GSO give the smallest FWHM for all positions. The FWHM at 25 cm from the center for LuI_3 is about 50% worse than the best scintillators. $RbGd_2Br_7$, $LaBr_3$, and BaF_2 have a factor of 2 worse spatial resolution at 25 cm than the best scintillators. Finally, $LaCl_3$ and NaI have resolutions that are 2.5 times worse than the best scintillators.

Despite the promising new materials, the ideal scintillator has not yet been discovered. TOF PET would benefit enormously from new scintillators that combine high light output and short decay time (to obtain excellent timing resolution), high density and effective atomic number (to obtain excellent spatial resolution and efficiency), and good linearity (to obtain excellent energy resolution).

3.2. Photomultiplier tubes

As the fast emissions from BaF_2 are in the UV region, TOF PET cameras in the 1980s required (expensive) quartz-windowed PMTs and optical glues (to couple the scintillator to the PMT) with poor mechanical properties. The new scintillators emit in the 400 nm range, allowing the use of (inexpensive) borosilicate glass-windowed PMTs. There has also been steady progress in PMTs over the past few decades. The general timing properties (especially the transit time jitter) of inexpensive, 25 mm diameter PMTs that also have the required energy resolution and stability have improved dramatically.

However, more improvements are necessary. Many of the PMTs that are used in commercial PET cameras have transit times that vary significantly across the face of the PMT [42]. In addition, the mean transit time varies from PMT to "identical" PMT. As most PET cameras use "block" detector modules that share light among multiple (usually four) PMTs, methods are needed to remove or correct for transit time differences between PMTs.

3.3. Electronics

The electronics available in the 1980s severely handicapped TOF PET. At that time, a fast personal computer had a clock speed of about 8 MHz. Digital electronics operating in the GHz range were virtually unheard of, as were custom application specific integrated circuits (ASICs). The timing circuitry was predominantly analog and tended to drift with both time and temperature. Thus, while 500 ps resolution could be obtained immediately after calibration, the camera rapidly went out of calibration and the timing resolution degraded. Digital logic operating in the GHz range is now routine, ASICs are commonplace, and the timing stability is outstanding. These improvements have also enabled the resurgence of TOF PET.

However, more improvements are necessary. One of the critical parts is an ASIC implementation of a constant fraction discriminator (CFD), or some other circuit that converts the analog pulse from the PMT into a digital timing pulse with high accuracy. A true CFD uses an analog delay line with frequency response of $\sim$10 GHz, and these are difficult to incorporate into an ASIC. Non-delay line CFD ASICs have been developed [32,43,44], but it is not clear whether these have the requisite timing accuracy. In addition, such an ASIC needs to include a high precision TDC and the rest of the electronic circuitry needed for a PET camera (gain adjustment, energy windowing, crystal identification, event formatting, test pulsing, etc.).

3.4. Detector module design

The shape of the scintillator crystal influences the achievable timing resolution. The exceptional numbers presented in Table 1 are generally obtained with small, flat scintillator crystals with the largest face coupled to the PMT. This geometry reduces the path length between the origin of the scintillation light and the photodetector and also maximizes the light collection efficiency. Conventional PET detector modules, on the other hand, have long, thin crystals whose smallest face is coupled to the PMT. In addition, the scintillation light is spread by a light guide, which increases the path length of the scintillation photons. This degrades the timing resolution. Current detector modules have not been optimized for timing resolution (at least not the sub-ns resolution needed by TOF PET), and additional effort is needed to develop geometries optimized for TOF PET.

3.5. Photodetectors

Timing resolution scales like the square root of the number of photons that are detected. One-to-one scintillator crystal to photodetector coupling generally increases the light collection efficiency (often by a factor of almost 2) compared to a block detector design. Current PMTs have quantum efficiencies of 25–30%. Thus, inexpensive photodetectors that are compact, pixellated, and have fast rise

time, low transit time jitter, and high QE (close to 100%) could improve the timing resolution by a factor of approximately 2. There are several promising new photodetector technologies, notably SiPM-type devices, that show potential for providing this.

3.6. Reconstruction algorithms

TOF reconstruction algorithms presently take more than an hour on Beowulf-type clusters and so must be sped up. Algorithms for correcting for Compton scatter and random events in TOF cameras are also needed.

Finally, evaluating the benefits of TOF is difficult. While estimates of variance reduction using filtered backprojection in uniform objects are relatively easy to obtain, the convergence properties of 3D iterative algorithms (which are the clinical standard today) make even this assessment difficult. In addition, we need methods for evaluating the TOF benefit in heterogeneous objects (such as patients) with varying amounts of scatter and random background. Most importantly, the clinical effectiveness must be evaluated. While it is relatively easy to quantitatively measure the improvement in signal-to-noise ratio in a simple phantom (e.g., a uniform cylinder with a central hot spot), it is much more difficult to quantitatively predict how the noise reduction affects diagnostic accuracy, especially as the noise reduction will depend on the activity distribution in the patient, and so has considerable variation.

4. Conclusions

TOF PET offers a significant reduction in statistical variance. Simple estimates predict a factor of ~5 variance reduction for realistic clinical imaging situations (35 cm diameter and 500 ps FWHM timing resolution). Such systems were developed in the 1980s, but failed because of deficiencies in the technologies available at that time. In the subsequent two decades, improved PMTs, electronics, and especially scintillators have become available and have lead to a recent rebirth in TOF PET. However, further developments in all of these technologies will further improve the effectiveness of this technique.

Acknowledgments

This work was supported in part by the Director, Office of Science, Office of Biological and Environmental Research, Medical Science Division of the US Department of Energy under contract no. DE-AC02-05CH11231, and in part by the National Institutes of Health, National Institute of Biomedical Imaging and Bioengineering under grant no. R33-EB001928.

References

[1] M.M. Ter-Pogossian, D.C. Ficke, M. Yamamoto, J.T. Hood, Design characteristics and preliminary testing of Super-PETT I, a positron emission tomograph utilizing photon time-of-flight information (TOF PET). in: Proceedings of The Workshop on Time of Flight Tomography, St. Louis, MO, 1982, pp. 37–41.
[2] M.M. Ter-Pogossian, D.C. Ficke, M. Yamamoto, J.T. Hood, IEEE Trans. Med. Imaging MI-1 (1982) 179.
[3] N.A. Mullani, W.H. Wong, R.K. Hartz, K. Yerian, E.A. Philippe, et al., Design of TOFPET: a high resolution time-of-flight positron camera. in: Proceedings of The Workshop on Time of Flight Tomography, St. Louis, MO, 1982, pp. 31–36.
[4] R. Gariod, R. Allemand, E. Cormoreche, M. Laval, M. Moszynski. The LETI positron tomograph architecture and time of flight improvements. in: Proceedings of The Workshop on Time of Flight Tomography, St. Louis, MO, 1982, pp. 25–29.
[5] W.H. Wong, N.A. Mullani, E.A. Phillipe, R. Hartz, K.L. Gould, J. Nucl. Med. 24 (1983) 52.
[6] T.K. Lewellen, A.N. Bice, R.L. Harrison, M.D. Pencke, J.M. Link, IEEE Trans. Nucl. Sci. NS-35 (1988) 665.
[7] B. Mazoyer, R. Trebossen, C. Schoukroun, B. Verrey, A. Syrota, et al., IEEE Trans. Nucl. Sci. NS-37 (1990) 778.
[8] M.M. Ter-Pogossian, D.C. Ficke, D.E. Beecher, G.R. Hoffmann, S.R. Bergmann, J. Comput. Assist. Tomogr. 18 (1994) 661.
[9] M.E. Casey, R. Nutt, IEEE Trans. Nucl. Sci. NS-33 (1986) 460.
[10] T.K. Lewellen, Semin. Nucl. Med. 28 (1998) 268.
[11] J.S. Robertson, R.B. Marr, M. Rosenblum, V. Radeka, Y.L. Yamamoto, 32-Crystal positron transverse section detector, in: G.S. Freedman (Ed.), Tomographic Imaging in Nuclear Medicine, Society of Nuclear Medicine Press, New York, 1973.
[12] M.M. Ter-Pogossian, M.E. Phelps, E.J. Hoffman, N. Mullani, Radiology 114 (1975) 89.
[13] H.O. Anger, ISA Trans. 5 (1966) 311.
[14] R.E. Campagnolo, P. Garderet, J. Vacher, Tomographie par emetreurs positrons avec mesure de temp de vol, in: Communication an Colloque National sur le Traitement du Signal, Nice, France, 1979.
[15] D.L. Snyder, L.J. Thomas, M.M. Ter-Pogossian, IEEE Trans. Nucl. Sci. NS-28 (1981) 3575.
[16] T. Tomitani, IEEE Trans. Nucl. Sci. NS-28 (1981) 4582.
[17] C.L. Melcher, J.S. Schweitzer, IEEE Trans. Nucl. Sci. NS-39 (1992) 502.
[18] W.W. Moses, M. Ullisch, IEEE Trans. Nucl. Sci. NS-53 (2006) 1.
[19] M. Moszynski, M. Kapusta, A. Nassalski, T. Szczesniak, D. Wolski, et al., New prospects for time-of-flight PET with LSO scintillators. in: B. Yu (Ed.), Proceedings of The IEEE 2005 Nuclear Science Symposium, San Juan, Puerto Rico, 2005, pp. J3-18.
[20] E.V.D. van Loef, P. Dorenbos, C.W.E. van Eijk, K. Kramer, H.U. Gudel, Appl. Phys. Lett. 79 (2001) 1573.
[21] S. Surti, J.S. Karp, L.M. Popescu, M.E. Daube-Witherspoon, M. Werner, Investigation of image quality and NEC in a TOF-capable PET scanner. in: A. Siebert (Ed.), Proceedings of The IEEE 2004 Nuclear Science Symposium, Rome, Italy, 2004, pp. M10-276.
[22] A. Kuhn, S. Surti, J.S. Karp, P.S. Raby, K.S. Shah, et al., IEEE Trans. Nucl. Sci. NS-51 (2004) 2550.
[23] A. Kuhn, S. Surti, J.S. Karp, G. Muehllehner, F.M. Newcomer, et al., Performance assessment of pixellated LaBr3 detector modules for TOF PET. in: A. Siebert (Ed.), Proceedings of The IEEE 2004 Nuclear Science Symposium, Rome, Italy, 2004, pp. M9-59.
[24] S. Surti, J.S. Karp, G. Muehllehner, Phys. Med. Biol. 19 (2004) 4593.
[25] J.S. Karp, A. Kuhn, A.E. Perkins, S. Surti, M.E. Werner, et al., Characterization of a time-of-flight PET scanner based on lanthanum bromide. in: B. Yu (Ed.), Proceedings of The IEEE 2005 Nuclear Science Symposium, San Juan, Puerto Rico, 2005, pp. M4-8.
[26] J. Glodo, W.W. Moses, W. Higgins, E.V.D. van Loef, P. Wong, et al., IEEE Trans. Nucl. Sci. NS-52 (2004) 1805.
[27] K.S. Shah, J. Glodo, W. Higgins, E.V.D. van Loef, W.W. Moses, et al., IEEE Trans. Nucl. Sci. NS-52 (2004) 3157.
[28] K.S. Shah, J. Glodo, M. Klugerman, W. Higgins, T. Gupta, et al., IEEE Trans. Nucl. Sci. NS-51 (2004) 2302.

[29] A. Kuhn, S. Surti, K.S. Shah, J.S. Karp, Investigation of $LaBr_3$ detector timing resolution. in: B. Yu (Ed.), Proceedings of The IEEE 2005 Nuclear Science Symposium, San Juan, Puerto Rico, 2005, pp. M7-122.
[30] M. Moszynski, T. Ludziejewski, D. Wolski, W. Klamra, V.V. Avdejcikov, Nucl. Instr. and Meth. A 188 (1981) 403.
[31] S.E. Derenzo, R.H. Huesman, J.L. Cahoon, A.B. Geyer, W.W. Moses, et al., IEEE Trans. Nucl. Sci. NS-35 (1988) 659.
[32] D.M. Binkley, Development and analysis of non-delay-line constant fraction discriminator circuits, including a fully-monolithic CMOS implementation, Ph.D. Thesis, University of Tennessee, Knoxville, 1992.
[33] J. Bialkowski, M. Moszynski, D. Wolski, W. Klamra, Nucl. Instr. and Meth. A 281 (1989) 657.
[34] S.I. Ziegler, H. Ostertag, W.K. Kuebler, W.J. Lorenz, E.W. Otten, IEEE Trans. Nucl. Sci. NS-37 (1990) 574.
[35] K. Ishii, S. Watanuki, H. Orihara, M. Itoh, T. Matsuzawa, Nucl. Instr. and Meth. A 253 (1986) 128.
[36] M. Moszynski, R. Allemand, M. Laval, R. Odru, J. Vacher, Nucl. Instr. and Meth. 205 (1983) 239.
[37] M. Moszynski, T. Ludziejewski, D. Wolski, W. Klamra, V.V. Avdejcikov, Nucl. Instr. and Meth. A 372 (1996) 51.
[38] M. Conti, B. Bendriem, M. Casey, M. Chen, F. Kehren, et al., Implementation of time-of-flight on CPS HiRez PET scanner. in: A. Siebert (Ed.), Proceedings of The IEEE 2004 Nuclear Science Symposium, Rome, Italy, 2004, pp. M3-1.
[39] M. Moszynski, D. Wolski, T. Ludziejewski, M. Kapusta, A. Lempicki, et al., Nucl. Instr. and Meth. A 385 (1997) 123.
[40] K.S. Shah, J. Glodo, M. Klugerman, W.W. Moses, S.E. Derenzo, et al., IEEE Trans. Nucl. Sci. NS-50 (2003) 2410.
[41] W.W. Moses, K.S. Shah, Nucl. Instr. and Meth. A 537 (2005) 317.
[42] M. Aykac, F. Bauer, C.W. Williams, M. Loope, M. Schmand, IEEE Trans. Nucl. Sci. NS-53 (2006) 1084.
[43] B.K. Swann, J.M. Rochelle, D.M. Binkley, B.S. Puckett, B.J. Blalock, et al., IEEE Trans. Nucl. Sci. NS-50 (2003) 909.
[44] D.M. Binkley, M.L. Simpson, J.M. Rochelle, IEEE Trans. Nucl. Sci. NS-38 (1991) 1754.